ACS APPLIED MATERIALS & INTERFACES

Letter

www.acsami.org

Amorphous Cobalt Hydroxide with Superior Pseudocapacitive Performance

H. B. Li,[†] M. H. Yu,[‡] X. H. Lu,[‡] P. Liu,[†] Y. Liang,[†] J. Xiao,[†] Y. X. Tong,*[,‡] and G. W. Yang*[,†]

[†]State Key Laboratory of Optoelectronic Materials and Technologies, Nanotechnology Research Center, School of Physics & Engineering, and [‡]MOE Key Laboratory of Bioinorganic and Synthetic Chemistry, School of Chemistry and Chemical Engineering, Sun Yat-sen University, Guangzhou 510275, Guangdong, P. R. China

ABSTRACT: Cobalt hydroxide ($Co(OH)_2$) has received extensive attention for its exceptional splendid electrical properties as a promising supercapacitor electrode material. $Co(OH)_2$ study so far prefers to crystal instead of amorphous, in spite of amorphous impressive electrochemical properties including the ability to improve the electrochemical efficiency based on the disorder structure. The amorphous $Co(OH)_2$ nanostructures with excellent electrochemical behaviors were successfully synthesized by a simple and green electrochemistry. Our as-prepared $Co(OH)_2$ electrode exhibited ultrahigh capacitance of 1094 F g^{-1} and super long cycle life of 95% retention over 8000 cycle numbers at a nominal 100 mV s^{-1} scan rate. The united pseudo-capacitive performances of the amorphous $Co(OH)_2$ nanostructures in electrochemical capacitors are totally comparable to those of the crystalline $Co(OH)_2$ nanomaterials. These findings actually open a door to applications of amorphous nanomaterials in the field of energy storage as superior electrochemical pseudocapacitors materials.

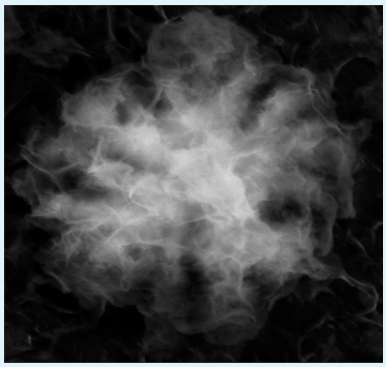

KEYWORDS: *amorphous cobalt hydroxide, electrochemical performance, high capacitance, super long-life*

With the continuous growth of demand for energy, there is an urge to develop new type of energy storage devices with high power and energy density.[1,2] Supercapacitors or electrochemical capacitors, as a new type of energy storage devices, have stimulated considerable interest recently for their desirable properties including short charging time, super-long cyclic lifetime, high power density, and low maintenance cost.[3−8] Considering the charge storage mechanism of supercapacitors, two kinds can be determined, one is electrical double-layer capacitors (EDLCs) and the other is pseudocapacitors.[6] Although EDLCs such as carbon-based EDLCs have long-term electrochemical stability, their charge mechanism limits their specific capacitances in a range of low values (lower than 300 F g^{-1}).[9] Contrarily, pseudocapacitors exhibit higher specific capacitances through surface redox reactions.[10−17] Excellent redox reaction capability of electrochemical electrode materials can improve the performance of energy storage device. Transition metal hydroxides such as cobalt hydroxide ($Co(OH)_2$) have attracted intensive attention to investigating the performance of crystalline nanomaterials with three-dementional architectures as advanced pseudocapacitors materials.[10−14] However, electrode materials with amorphous phase are usually evaluated to be unsuitable for electrochemical capacitors because of poor performance.[15,16] As a matter of fact, amorphous nanomaterials have rather unique electrochemical behaviors.[17] In this contribution, the amorphous $Co(OH)_2$ nanostructures have been fabricated by a simple, facile, green, and low-cost electrochemistry technique,[18] and the amorphous $Co(OH)_2$ electrochemical behaviors have been investigated. Interestingly, our measurements demonstrate that our as-prepared amorphous $Co(OH)_2$ nanostructures exhibit excellent electrochemical performances with ultrahigh capacitance (1094 F g^{-1}) and super-long cyclic lifetime (95% retention over 8000 cycle numbers), which are totally commensurate with that of its crystalline phase materials. Thus, these results substantiate amorphous nanomaterials applications as advanced electrochemical pseudocapacitor materials.

The amorphous $Co(OH)_2$ nanostructures are synthesized on a graphite flake (10 × 10 mm in size) by a unique electrochemistry technique in high-purity deionized water without any chemical additives.[18] A pure cobalt target is placed on the center of a chamber bottom. The fabrication is carried out in a constant voltage of 100 V for 1.5 h and the fabrication is performed at room temperature. Before the experiment, the cobalt target and graphite flakes should be cleaned with ethanol and water several times. The detail experiment and the formation mechanism can be seen in our previous paper.[17]

The structural properties of the amorphous cobalt hydroxide electrode materials are characterized by field-emission scanning electron microscopy (SEM) (JSM-6330F), transmission electron microscopy (TEM) and selected area electron diffraction (SEAD) (JEM2010-HR, 200 KV), X-ray photoelectron spectroscopy (XPS) (ESCALab250, Thermo VG), IR spectroscopy (EQUINOX 55), and Raman spectroscopy (Renishaw inVia). We can calculate the mass of prepared samples according to the gravimetric cobalt, which can be measured by inductively coupled plasma-atomic emission

Received: October 28, 2013
Accepted: January 2, 2014
Published: January 3, 2014

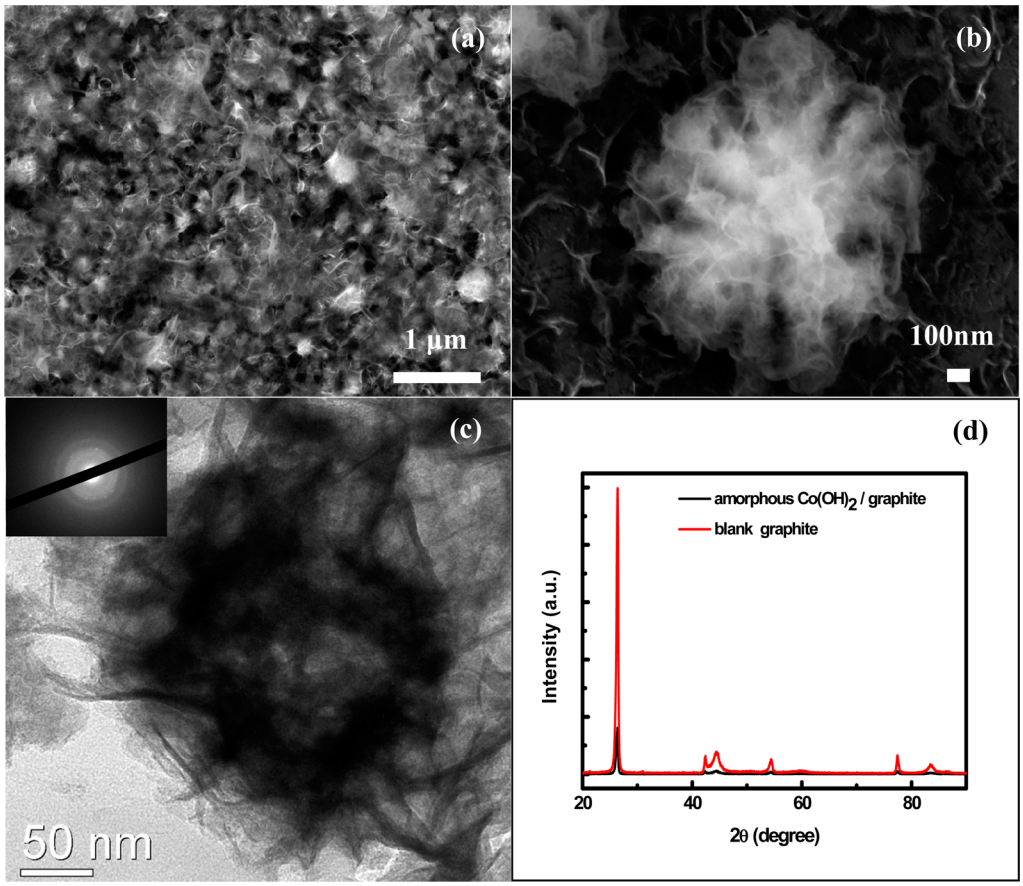

Figure 1. (a, b) SEM images of the as-synthesized amorphous $Co(OH)_2$ nanostructures on graphite electrodes, (c) TEM images of the sample and the corresponding SAED pattern, and (d) XRD patterns of the products.

spectrometry (TJA, IRIS-DUO-HR). Cyclic voltammetry (CV) and galvanostatic charging/discharging tests are carried out on a CHI 660D electrochemical workstation in a three-electrode system to characterize the electrochemical capabilities of our amorphous $Co(OH)_2$ electrode. A Pt foil and a saturated calomel electrode (SCE) are treated as counter electrode and reference electrode, respectively. The electrochemical tests are conducted in 1 M KOH solution.

A typical SEM image with low-magnification in Figure 1a shows the entire surface of our as-synthesized sample. From the SEM image with high magnification in Figure 1b, we can see a single flowerlike particle with diameter of about 500 nm and a wrinkled surface. In other words, the as-synthesized nanoparticles possess a three-dimensional surface. Further morphological characterizations of the flowerlike nanoparticles are carried out by high-resolution TEM (HRTEM). As shown in Figure 1c, HRTEM images reveal high-density wrinkled surfaces. The inset of Figure 1c, the corresponding SEAD pattern taken from the areas in Figure 1c, shows a broad and diffused halo ring, definitely suggesting an amorphous phase. In addition, X-ray diffraction (XRD) pattern is used to characterize the structure of the as-synthesized sample. Figure 1d shows the XRD patterns of as-prepared samples (black line) and the blank graphite substrate (red line), which reveals no proof for a crystalline phase since no other extra peaks appeared in the XRD of $Co(OH)_2$/graphite.

XPS, a reliable technique, is usually used to investigate the atoms chemical states of material surface by measuring the binding energy. In our case, XPS is used to study the chemical states of compounds. Figure 2a shows the complete survey XPS spectrum of the as-prepared sample. Three main peaks, C 1s, O 1s, and Co 2p, are exhibited in the spectrum. These results thus suggest our prepared sample is pure without chemical contaminations. The peaks located at 284.5 and 531.5 eV can be attributed to the characteristic of C 1s and O 1s representing the bound hydroxide groups (OH^-), corresponding to the previously reported works.[19−21] The high-resolution XPS spectra of Co 2p the sample is shown in the inset of Figure 2a. Two binding energies located at 781.12 and 786.3 eV in the Co 2p XPS spectra correspond to Co 2p3/2, yielding a characteristic of the Co^{2+} state, which matches with the previous reference.[19] Therefore, XPS spectroscopy studies reveal the $Co(OH)_2$ phase formation with amorphous nanostructure.

To further confirm the XPS analysis, we examined the composition of the as-synthesized sample by Raman spectra in the range of 100−1000 cm^{-1} (Figure 2b). Clearly, six broad peaks located at 191, 463, 482, 519, 579, and 689 cm^{-1} can be found. These peaks are in agreement with those reported by Yang et al.[19] The strongest band at 519 cm^{-1} is due to vibrations of the Co−O (A_g) symmetric stretching mode.[19,22] In addition, the band of 579 cm^{-1} corresponding to the Co−O stretching mode is broadened comparing with the crystalline phase[19] since disorder structures within the amorphous phase. The bands at 463 and 482 cm^{-1} can be attributed to an O−Co−O bending mode. Furthermore, the 463 cm^{-1} peak can be observed at 431 cm^{-1} in the IR spectrum (Figure 2c). The peaks of 689 and 191 cm^{-1} can be attributed to the A_{1g} and E_g

dx.doi.org/10.1021/am404769z | ACS Appl. Mater. Interfaces 2014, 6, 745−749

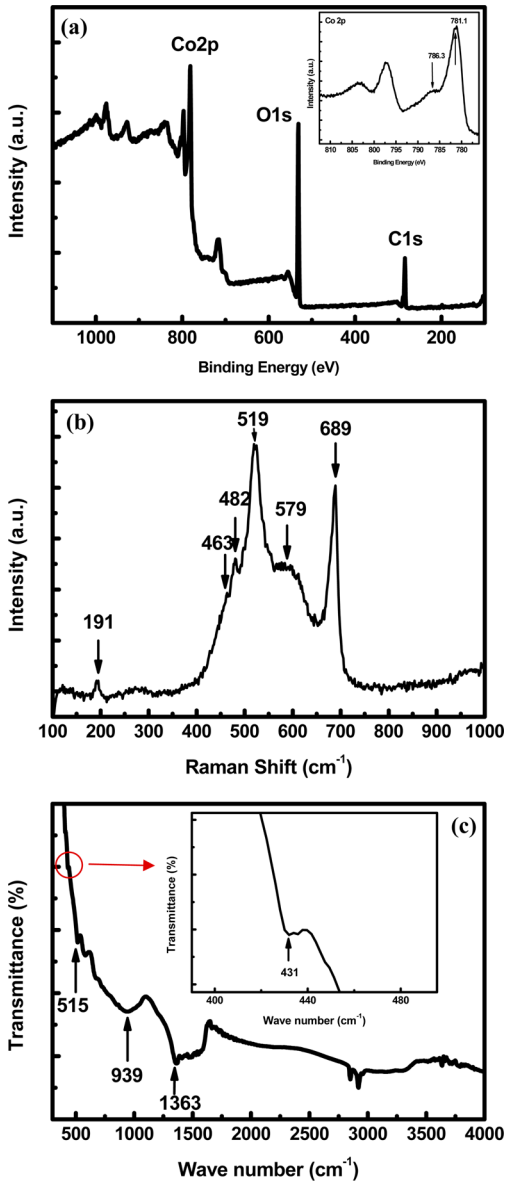

Figure 2. (a) XPS spectra and corresponding high-resolution XPS spectra of Co 2p and (b) Raman and (c) IR spectra of the amorphous $Co(OH)_2$ nanostructures.

mode, respectively. Compared with the crystalline phase, the bands of amorphous $Co(OH)_2$ are broaden and shifted with a small range. A large number of disorder and defects are distributed in the amorphous $Co(OH)_2$, and the disorders and defects can be result in Raman band shifts.

IR spectroscopy is carried out over a range of 400−4000 cm^{-1} to further verifies the chemical species of the amorphous sample. The IR spectrum of our prepared samples (Figure 2c) displays some peaks at 431, 515, 582, 939, 1363, 2850, and 2919 cm^{-1}. The bands located at 431 and 939 cm^{-1} are due to an in-plane Co−O−H bending vibration and OH deformation mode, respectively. The bands of 515 and 582 cm^{-1} are attributed to Co−O stretching vibrations.[19] The 1363 cm^{-1} band is assigned to the vibration $\nu_{C=O}$ of the absorbed CO_2 molecules.[19] Those bands are shifted and broadened due to the amorphous phase containing lots of disorder and defects. The 2919 and 2850 cm^{-1} may be caused by the infrared active vibrations of the absorbed H_2O.[23−25] On the basis of the above results and analysis, the amorphous $Co(OH)_2$ with flowerlike nanostructures are fabricated successfully in our work.

To investigate the charge storage mechanism and electrochemical performance of the as-synthesized amorphous $Co(OH)_2$ nanostructures, we employed cyclic voltammetry (CV) measurement in alkaline electrolyte with a three-electrode system. Typical CV curves for the amorphous $Co(OH)_2$ electrode at a series of scan rates (1−100 mV s^{-1}) with potential range of −0.2 to 0.4 V are presented in Figure 3a. It

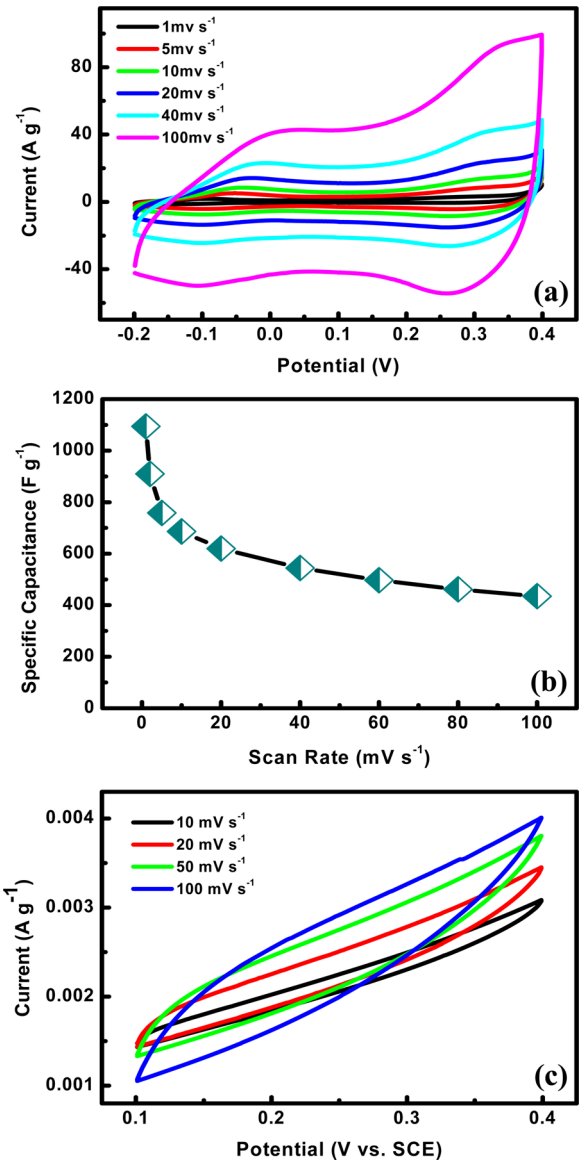

Figure 3. (a) CV curves, (b) specific capacitance of the amorphous $Co(OH)_2$ nanostructures, and (c) CV curves of the blank electrode at various scan rates.

can be easily found that CV curves contain two pairs of prominent redox peaks. The curves' shape suggests that the capacitance of amorphous $Co(OH)_2$ is faradic pseudocapacitance, produced by the redox reactions near the electrode surface. For electric double-layer capacitance, produced by the charge separation at the interface between electrolyte and electrode, the shape of CV curve would be close to rectangular. High redox current and obvious redox peaks imply excellent pseudocapacitive behavior for the amorphous $Co(OH)_2$

dx.doi.org/10.1021/am404769z | ACS Appl. Mater. Interfaces 2014, 6, 745−749

electrode. According to the literature, Faradaic redox reactions occurring on the surface of $Co(OH)_2$ electrode can be described as follows[13,14,26]

$$Co(OH)_2 + OH^- \leftrightarrow CoOOH + H_2O + e^-$$

$$CoOOH + OH^- \leftrightarrow CoO_2 + H_2O + e^- \quad (1)$$

The characteristic symmetric of the anodic and cathodic peaks suggests excellent electrochemical reversibility for $Co(OH)_2$ nanostructures as active electrode. It can be easily found that the CV curves perform little alteration in shape with increasing scan rate, which suggests excellent electron conduction within nanoparticles. As the scan rate increased, the cathodic and anodic peaks shifted in more negative and positive potential as a consequence of the internal resistance of the electrode. We can estimate the specific capacitance C (F g^{-1}) by the following formula[27]

$$C = \frac{1}{m\nu(V_c - V_a)} \int_{V_a}^{V_c} I(V)dV \quad (2)$$

where υ (mV s^{-1}) is the potential scan rate, m (g) is the active material mass, I (A) is the response current density, and V_a (V) and V_c (V) are the starting and ending potential, respectively. The $Co(OH)_2$ nanostructures are deposited on the graphite substrate with a loading density of 0.124 mg cm^{-2}. Thus, the specific capacitance at a scan rate of 1 mV s^{-1} is estimated to be 1094 F g^{-1}. When the scan rate increases to 100 mV s^{-1}, the obtained specific capacitance is 435.4 F g^{-1}, which represents only a 60% decrease of that at a low scan rate of 1 mV s^{-1}. A series of specific capacitances calculated from CV curves of Figure 3a are presented in Figure 3b. It can be easily found that the capacitance is negative correlated with the scan rate, i.e., the capacitance increases with the decrease of the scan rate. The as-prepared amorphous $Co(OH)_2$ exhibits excellent electrochemical performance with high-rate competence and high capacitance. This phenomenon is caused by the limitation of the electrolytic ions diffusion and migration within the active electrode effectively at high scan rates.[17] Moreover, the capacitance obtained in our work is higher than that of the reported crystalline $Co(OH)_2$ nanomaterials such as graphene-$Co(OH)_2$ nanocomsites (972.5 F g^{-1})[28] and $Co(OH)_2$ nanowire (624.5 F g^{-1}).[29]

Figure 3c displays the electrochemical behaviour of blank graphite electrode without any samples deposited. The current density of the graphite is about ~0.004A g^{-1}. Compared with the value of ~90 A g^{-1} produced by the amorphous $Co(OH)_2$/graphite electrode, the value of ~0.004A g^{-1} can be neglected. In other words, the magnified capacitance resulting from the graphite substrate (0.180 g cm^{-2}) can be ignored.

The galvanostatic charge−discharge measurement is another dependable technique to investigate the electrochemical capacitive behaviour. Figure 4a illustrates the charging-discharging curves of the amorphous $Co(OH)_2$ nanostructures at various current densities (16.7 to 50 A g^{-1}) with a potential widow from −0.2 to 0.4 V. It can be easily found that charging curve is in nearly symmetrical relationship with its corresponding discharging curve, which implies the excellent reversibility. These results thus substantiate the result of the CV curves. The specific capacitance can be estimated by the following equation[13]

$$C = \frac{1\Delta t}{m\Delta V} \quad (3)$$

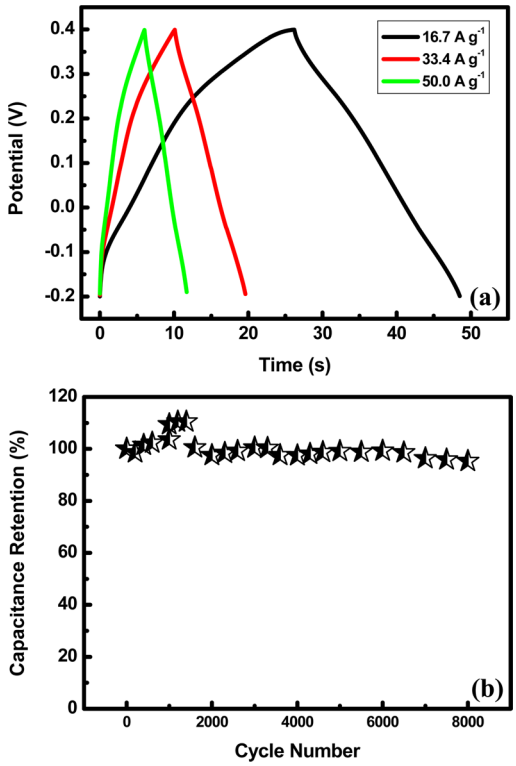

Figure 4. (a) Charge−discharge curves of the amorphous $Co(OH)_2$ nanostructures at various current densities (ranging from 16.7 to 50 A g^{-1}) and (b) cycle performance of the amorphous $Co(OH)_2$ sample measured at a scan rate of 100 mV s^{-1} for 8000 cycles.

where ΔV (V), m (g), Δt (s), and I(A) are the potential drop during discharge, active material mass, discharge time and discharge current, respectively. The specific capacitances calculated from the charge-discharge curves (Figure 4a) are 621, 512, and 475 F g^{-1} at 16.7, 33.4, and 50 A g^{-1}, respectively. It can be easily concluded that the capacitance is in negative correlation with the current density.

Taking account of the superior cycling stability, a requirement for high-performance electrochemical capacitors, a cycle-life measurement was performed on our amorphous $Co(OH)_2$ electrode. The cycle capability of our $Co(OH)_2$ sample at 100 mV s^{-1} scan rate for 8000 cycle numbers are presented in Figure 4b. Afterwards, the specific capacitance loss after 8000 consecutive cycles is negligible (about 5% loss), which indicates an superior long-term cycling-life for our amorphous $Co(OH)_2$ sample. Additionally, this value is highly comparable to that of the reported crystalline $Co(OH)_2$ materials.[13,14]

Thus, these results above demonstrate that the amorphous $Co(OH)_2$ nanomaterials are promising materials as positive electrode in electrochemical pseudocapacitor because of their high specific capacitance and excellent electrochemical stability.

We consider the following reasons for the amorphous $Co(OH)_2$ nanostructures having excellent electrochemical properties because the electronic conductivity and surface structure of materials impact their electrochemical capabilities. The first point is the pure surface of our as-prepared samples, which can make $Co(OH)_2$ interact with electrolytes effectively. The next point is that the three-dimensional surfaces for these nanostructures present a larger specific surface area than that of the smooth nanospheres. High specific surface area can help electrolytic ions in solution to be adsorbed on the electrode.

dx.doi.org/10.1021/am404769z | ACS Appl. Mater. Interfaces 2014, 6, 745−749

The third point is the amorphous structures. In fact, the disorder structures in cobalt hydroxide could greatly improve the electrochemical efficiency.[30] Additionally, a material having poor crystallinity or amorphous phase may result in more transportation channels than that of a highly crystalline one. Lastly, the flowerlike $Co(OH)_2$ nanostructures are self-assembled on the graphite substrate directly, which can lead to splendid electrical conductivity between nanoparticles and the substrate, and that is favorable to the electrolytic ions diffusion and migration.

In conclusion, we have successfully fabricated the amorphous cobalt hydroxide nanostructures with three-dimensional surface structure by a simple and green electrochemical approach, and demonstrated that the as-prepared amorphous cobalt hydroxide nanostructures possess excellent electrochemical performance with ultrahigh specific capacitance and super-long cycle life as promising positive electrode materials for pseudosupercapacitors. Importantly, their integrated electrochemical performances in supercapacitors are totally commensurate with those of the cobalt hydroxide materials with crystalline phase. Therefore, the results in our study actually open the door to applications of the amorphous $Co(OH)_2$ nanomaterials in constructing high-performance electrochemical capacitors as well as other energy storage devices.

AUTHOR INFORMATION

Corresponding Authors

*E-mail: stsygw@mail.sysu.edu.cn.
*E-mail: chedhx@mail.sysu.edu.cn

Notes

The authors declare no competing financial interest.

ACKNOWLEDGMENTS

The National Basic Research Program of China (2014CB931700) and State Key Laboratory of Optoelectronic Materials and Technologies supported this work.

REFERENCES

(1) Niu, Z.; Dong, H.; Zhu, B.; Li, J.; Hng, H. H.; Zhou, W.; Chen, X.; Xie, S. *Adv. Mater.* **2013**, *25*, 1058−1064.
(2) El-Kady, M. F.; Strong, V.; Dubin, S.; Kaner, R. B. *Science* **2012**, *335*, 13261330.
(3) Winter, M.; Brodd, R. J. *Chem. Rev.* **2004**, *104*, 4245−4269.
(4) Miller, J. R.; Simon, P. *Science* **2008**, *321*, 651−654.
(5) Liu, D.; Zhang, Q.; Xiao, P.; Garcia, B. B.; Guo, Q.; Champion, R.; Cao, G. *Chem. Mater.* **2008**, *20*, 1376−1380.
(6) Lu, X. H.; Yu, M. H.; Wang, G. M.; Zhai, T.; Xie, S. L.; Ling, Y. C.; Tong, Y. X.; Li, Y. *Adv. Mater.* **2013**, *25*, 267−272.
(7) Lu, X. H.; Wang, G. M.; Zhai, T.; Yu, M. H.; Gan, J. Y.; Tong, Y. X.; Li, Y. *Nano Lett.* **2012**, *12*, 1690−1696.
(8) Yuan, L. Y.; Xiao, X.; Ding, T. P.; Zhong, J. W.; Zhang, X. H.; Shen, Y.; Hu, B.; Huang, Y. H.; Zhou, J.; Wang, Z. L. *Angew. Chem., Int. Ed.* **2012**, *51*, 4934−4938.
(9) Kaempgen, M.; Chan, C. k.; Ma, J.; Cui, Y.; Gruner, G. *Nano Lett.* **2009**, *9*, 1872−1876.
(10) Wang, H. L.; Casalongue, H. S.; Liang, Y. Y.; Dai, H. J. *J. Am. Chem. Soc.* **2010**, *132*, 7472−7477.
(11) Yan, J.; Fan, Z. J.; Sun, W.; Ning, G. Q.; Wei, T.; Zhang, Q.; Zhang, R. F.; Zhi, L. J.; Wei, F. *Adv. Funct. Mater.* **2012**, *22*, 2632−2641.
(12) Yang, G. W.; Xu, C. L.; Li, H. L. *Chem. Commun.* **2008**, *0*, 6537−6539.
(13) Choi, B. G.; Yang, M. H.; Jung, S. C.; Lee, K. G.; Kim, J. G.; Park, H. S.; Park, T. J.; Lee, S. B.; Han, Y. K.; Huh, Y. S. *ACS Nano* **2013**, *3*, 2453−2460.
(14) Cao, L.; Xu, F.; Liang, Y. Y.; Li, H. L. *Adv. Mater.* **2004**, *16*, 1853−1857.
(15) Hu, C. C.; Chen, J. C.; Chang, K. H. *J. Power Sources* **2013**, *221*, 128−133.
(16) Liu, C. J.; Li, Y. W. *J. Alloys. Compd.* **2009**, *478*, 415−418.
(17) Li, H. B.; Yu, M. H.; Wang, F. X.; Liu, P.; Liang, Y.; Xiao, J.; Wang, C. X.; Tong, Y. X.; Yang, G. W. *Nat. Commun.* **2013**, *4*, 1894.
(18) Li, H. B.; Liu, P.; Liang, Y.; Xiao; Yang, G. W. *Nanoscale* **2012**, *4*, 5082−5091.
(19) Yang, J.; Liu, H. W.; Martens, W. N.; Frost, R. L. *J. Phys. Chem. C* **2009**, *114*, 111−119.
(20) Amri, A.; Jiang, Z. T.; Pryor, T.; Yin, C. Y.; Xie, Z. H.; Mondinos, N. *Surf. Coat. Technol.* **2012**, *207*, 367−374.
(21) Payne, B. P.; Biesinger, M. C.; McIntyrea, N. S. *J. Electron Spectrosc. Related Phenom.* **2012**, *185*, 159−166.
(22) Shieh, S. R.; Duffy, T. S. *Phys. Rev. B* **2002**, *66*, 134301.
(23) Bantignies, J. L.; Deabate, S.; Righi, A.; Rols, S.; Hermet, P.; Sauvajol, J. L.; Henn, F. *J. Phys. Chem. C* **2008**, *112*, 2193−2210.
(24) Kim, S. J.; Park, G. J.; Kim, B. C.; Chung, J. K.; Wallace, G. G.; Park, S. Y. *Synth. Met.* **2012**, *161*, 2641−2646.
(25) Hermet, P.; Gourrier, L.; Bantignies, J. L.; Ravo, D.; Michel, T.; Deabate, S.; Boulet, P.; Henn, F. *Phys. Rev. B* **2011**, *84*, 235211.
(26) Svegl, F.; Orel, B.; Hutchins, M. G.; Kalcher, K. *J. Electrochem. Soc.* **1996**, *143*, 1532−1539.
(27) Srinivasan, V.; Weidner, J. W. *J. Power Sources* **2002**, *108*, 15−20.
(28) Chen, S.; Zhu, J. W.; Wang, X. *J. Phys. Chem. C* **2010**, *114*, 11829−11834.
(29) Jiang, J.; Liu, J. P.; Ding, R. M.; Zhu, J. H.; Li, Y. Y.; Hu, A. Z.; Li, X.; Huang, X. T. *ACS Appl. Mater. Interfaces* **2011**, *3*, 99−103.
(30) Bermard, M. C.; Cortes, R.; Keddam, M.; Takenouti, H.; Bernard, P.; Senyarich, S. *J. Power Source* **1996**, *63*, 247−254.